CHAPTER 32

Principles of Doppler OCT

Victor XD Yang, I Alex Vitkin

INTRODUCTION

Over the past decade, several new contrast mechanisms that supplement OCT microstructural imaging capability have been investigated. Of these, one of the most significant and physiologically relevant is the ability to detect tissue blood flow. This functional extension of OCT has become variously known as optical Doppler tomography, color Doppler OCT, or Doppler OCT (D-OCT); we will use the last term for simplicity. Despite the terminology, it is interesting to note that the classical Doppler effect (frequency shift of the reflected wave caused by the motion of the object) may not play a primary role in some methods of signal detection, as elaborated below. Since its first demonstrations in the mid-1990s[1–3], several research groups have worked intensely on using D-OCT to detect blood flow in tissues. Various methods of D-OCT flow detection have been explored, different experimental systems have been implemented and initial *in vivo* results in a variety of tissues have been obtained[4–12]. Most of these developments have utilized the time-domain OCT methods; very recently, both spectral and frequency domain OCT approaches have been adopted for D-OCT imaging as well[13–18].

This chapter briefly reviews the underlying physics of D-OCT, discusses Doppler image display modes, describes experimental implementation methods and highlights selected clinical demonstrations. As a case study example, a particular phase-sensitive time domain D-OCT system that has enabled microvascular blood flow detection in endoscopic and interstitial settings is presented in more detail. We conclude with a discussion of the future of this promising approach for simultaneous high-resolution real-time non-invasive imaging of tissue structure and function.

Initially investigated by the Austrian physicist Christian Johann Doppler in the mid-1800s, the effect named after its discoverer is a phenomenon whereby a moving sound source seems more highly pitched when approaching an observer, and of lower pitch when receding from one. This apparent shift in frequency also occurs when the source is stationary and the observer is moving, emphasizing the importance of the relative velocity between the two. Further, the effect can be generalized beyond sound to all types of wave phenomena, including electromagnetic radiation, as was done several years later in France by Armand Fizeau. The Doppler effect has been used extensively in many branches of science and engineering – for example in astronomy to quantify the approach and recession speeds of various interstellar and extragalactic objects (culminating in Hubble's formulation of the expanding universe). Closer to home, the most familiar use of the Doppler effect is in automobile radars that detect speeding motorists on local roads. In the biomedical arena, the past ~40 years have witnessed the utilization of the Doppler effect for non-invasive assessment of tissue blood flow. The most familiar examples of these biomedical Doppler techniques are laser Doppler flowmetry (LDF) and Doppler ultrasound imaging.

LDF, the traditional optical technique employed for microcirculation assessment in the clinical setting, has the advantage of being compatible with endoscopic (and intravascular) tissue access through to the use of fiberoptics[19]. This method employs monochromatic laser light, most commonly a frequency stabilized HeNe laser at 633 nm, to illuminate the tissue of interest. When photons are scattered back from moving red blood cells (RBCs), the frequency of the light is shifted due to the Doppler effect. By analyzing the spectral content change of the scattered light, this technique can detect flow velocities from 0.08 to over 1 mm/s[20], which is relevant to the speed of slow-moving RBCs in the capillary bed. However, multiple scattering of photons in tissue makes it extremely difficult to determine the scattering angle of each photon-to-RBC interaction, and thus

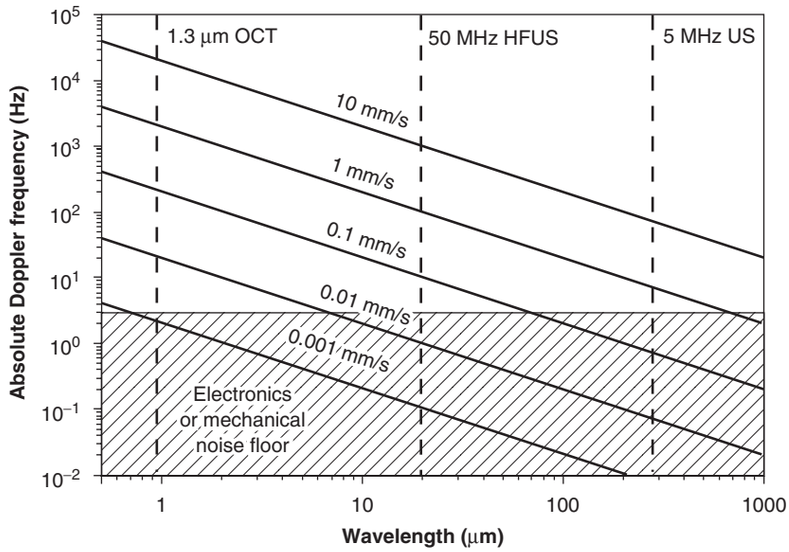

Figure 32.1 Schematic plot showing Doppler frequency induced by different flow velocities when using Doppler ultrasound at 5 and 50 MHz, in comparison to Doppler OCT at 1.3 μm (assuming the refractive index of tissue is 1.4, and a frequency independent detection noise floor of ~3 Hz)

LDF cannot provide the absolute measurement of RBC velocity (see Figure 32.2 and equation 2). Another problematic aspect of LDF is its inherent lack of depth resolution. Due to light scattering at this wavelength, the effective interrogation volume of LDF is about 1 mm^3, with a penetration depth on the order of hundreds of micrometers[21]. The LDF signal is the integral within this volume and the technique has no depth discrimination. Nevertheless, LDF (especially combined with optical beam scanning) remains an excellent tool for detecting relative blood flow changes in superficial tissues, such as the skin[22], retina[23], and gastrointestinal tract[24].

Doppler ultrasound (US), using frequencies ranging from approximately 2 to 15 MHz, is the most widely used clinical imaging modality for accessing the vasculature, typically targeting larger vessels such as the carotid. Various methods of assessing blood flow have been developed[25], as briefly described below, and various modes of data display are employed, typically involving an overlay of a selected blood flow Doppler map over the structural reflectivity (brightness or B-mode) image. The Doppler US displays are dynamic in nature, employing fast update (often real-time or video rates) visualizations, not static images common to other medical imaging modalities. This ability to provide the clinician with real-time visualization and guidance is particularly important for Doppler imaging, because tissue blood flow can be pulsatile, intermittent, rapidly changing and otherwise variable in time. The difference between dynamic imaging as seen in the clinical setting, and static image displays as reported in publications (and, for example, Chapter 14) must be borne in mind – Doppler US and Doppler OCT, as described below, are often more impressive and more valuable in their real-life environment.

In addition to its broad clinical acceptance, active research in Doppler US continues, particularly in extending its velocity sensitivity and spatial resolution to enable imaging of slower flows in smaller blood vessels. Advances in power Doppler[26], microbubble contrast agent[27] and broadband signal processing[28] are particularly noteworthy in this regard. In practice, it remains difficult to use Doppler US at clinical (~10 MHz) frequencies to detect blood flow slower than a few centimeters per second. By increasing the US frequency to reduce the interrogation wavelength, this situation can be improved (Figure 32.1). High-frequency ultrasound (HFUS) in the 40–100 MHz range, or ultrasound biomicroscopy (UBM), has been used to image tumor models in animal studies[29]. Doppler UBM systems can image the microcirculation and detect blood flow velocity on the order of a few millimeters per second in vessels as small as 20 μm in diameter[30]. In animal studies, it has been used for quantitative monitoring of the effect of antivascular therapy based on integrated Doppler power measurement within the imaged tumor volume[31]. The main practical difficulty in using this technology *in vivo* has been the lack of high-frequency multielement transducer arrays. As a result, single-element transducer systems have been used to make two-dimensional images in both B- and Doppler modes. Although real-time frame rates can be achieved in B-mode, the transducer lateral scanning speed must be sufficiently slow to avoid motion artifacts when operating in Doppler mode. Consequently, the frame rate in Doppler mode

cannot reach realtime*, which limits its use. A related difficulty in using UBM in endoscopic/intravascular applications is that catheter-based US probes typically use a single transducer, and thus suffer from the same problem.

TISSUE BLOOD FLOW AND THE DOPPLER EFFECT

The equation describing the Doppler effect states that the Doppler shift of waves scattered from a moving target is proportional to the frequency of the interrogating wave (and inversely proportional to its wavelength):

$$f_D = \frac{2V_z}{c - V_z} f_0 \approx \frac{2V_z}{c} f_0 = \frac{2V_z}{\lambda_0} \quad (1)$$

where f_D is the Doppler shift, V_z is the target velocity in the direction of the wave propagation which travels at c ($c \gg V_z$) with a frequency of f_0, and the wavelength is λ_0. From Figure 32.1, it is clear that, by using shorter waves such as infrared light at 1.3 μm (effective wavelength in tissue is approximately 0.9 μm due to tissue refraction index, which is assumed to be 1.4) flow velocities as slow as 2 μm/s can be measured . In addition, shorter wavelength also allows the light beam to be focused tighter than ultrasound, increasing spatial resolution and reducing the sampling volume to possibly smaller than a single capillary, which may permit detailed imaging of the microvasculature.

Extending the Doppler equation (1) to the case of arbitrary interrogation geometry represented by the Doppler angle θ (Figure 32.2), the Doppler frequency f_D of the blood flow, is proportional to the velocity:

$$f_D = \frac{2n_t V \cos\theta}{c} f_0 = \frac{2n_t V \cos\theta}{\lambda n} \quad (2)$$

where V is the blood flow velocity (= $V_z/\cos\theta$), f_0 is the center frequency of the broadband light, and n_t is the refractive index of tissue. When investigating the same flow velocity, using a 1.3 μm OCT system can elicit a Doppler frequency over two orders of magnitude higher than using 5MHz US. By using the shorter wavelength in the optical regimen, the Doppler signal from slow flow is raised above the noise floor and detected. The smaller fractional bandwidth of the OCT system also favors the identification of the Doppler frequency with enhanced accuracy[25].

A simple example will illustrate the relevant numbers inherent in Doppler imaging of tissues.

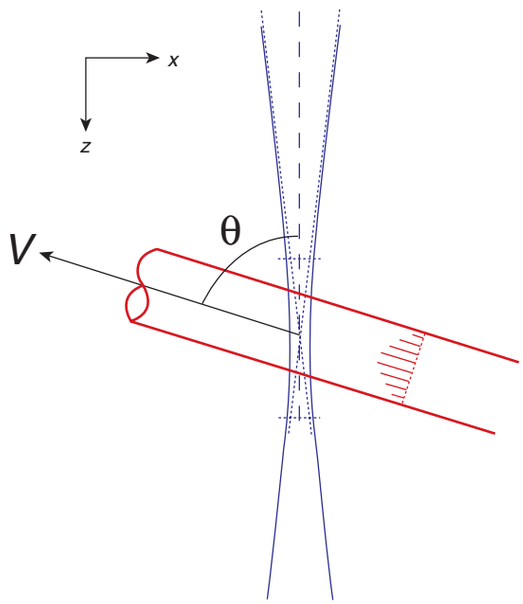

Figure 32.2 Coordinate system for blood flow (red) through the optical beam (blue)

Physiological blood flow velocities range from 10^{-6} to 10^{-2} m/s in the microcirculatory circuits (including capillaries, arterioles and venules) and can reach >1 m/s in the major vessels[32]. Assuming a perfusion-level blood flow velocity of 2 mm/s, tissue refractive index of 1.4, OCT center wavelength of 1300 nm and a Doppler angle of 60°, the OCT Doppler shift f_D is approximately 2.2 kHz (equation (2) and Figure 32.1). The same flow detected with a HFUS system (50 MHz, λ_o~23 μm) would yield a much lower US Doppler frequency shift of only ~130 Hz, owing to the longer US wavelength and the Doppler frequency's inverse dependence on it. This much smaller blood-flow-related frequency shift is harder to detect, and points to D-OCT's potential advantage in terms of minimum velocity resolution and sensitivity to slower (perfusion-level) blood flows. However, even with the higher f_D inherent in the optical approach, such frequency shifts represent tiny portions of the frequency bandwidth content of either OCT or pulsed-wave US systems, and considerable ingenuity (and often indirect methods) are required for accurate flow determination.

OCT METHODS TO DETECT PHYSIOLOGICAL DOPPLER SIGNALS

There are several approaches for detecting tissue blood flow using OCT, as described in the literature

*Among other parameters, the spatial resolution, lateral scanning speed, and minimum detectable velocity are related in Doppler UBM. For a typical 40 MHz UBM scanning an 8 mm wide image, and if the desired minimum detectable velocity resolution of 1 mm/s will yield a frame rate will be approximately 0.5 s^{-1}.

and reviewed in several book chapters[8,9]; the major ones will be briefly highlighted below. Arguably the most direct is to detect the true Doppler shift by analyzing the time-domain OCT data in Fourier (frequency) space, in order to distinguish the flow-induced modulation components superposed on the interferometric signal due to the (constant) reference arm velocity. The mean velocity of flowing scatterers (e.g. RBCs in blood vessels) as a function of depth is estimated from the computed centroid frequency of the local interferometric reflectance, by using overlapped short time Fourier transforms (ST-FT). Although computationally intensive and thus difficult to apply to *in vivo* dynamics, this allows an estimation of Doppler shifts along each scan line, which may be transformed to mean blood velocities if the Doppler angles are known. Considerations related to optimal selection of the time window for the ST-FT processing, the amount of overlap between adjacent windows, and trade-offs between improved velocity resolution and reduced imaging speeds in ST-FT methods have been extensively described and reviewed in the literature[2,8,9,33].

Another approach for OCT Doppler flow imaging is to detect the local (depth-resolved) phase change by comparing sequential or adjacent depth scans[3,34–36]. For example, one can determine the phase by performing the Hilbert transform on the OCT signal, and then obtain the Doppler shift by dividing the phase difference between two adjacent scans by the time between line acquisitions ($T_a = 1/[\text{A-scan rate}] = 1/f_a$). The potential advantages of such phase-based methods over the ST-FT approaches are that the velocity sensitivity and spatial resolution are not in direct opposition, and the computational requirements are lighter. Phase-based Doppler OCT imaging can also yield increased axial scanning speed, higher frame rates and reduced speckle noise[3,34–37]. Besides Hilbert-transform approaches, other methods of phase resolved Doppler OCT imaging are possible – for example, the Kasai flow estimator as described in greater detail below.

Before proceeding to a particular illustrative example of phase resolved Doppler OCT imaging, it should be noted that, besides the ST-FT and phase methods, several other means of OCT flow detection are possible. These include Doppler broadening and shift approaches that permit the estimation of the total velocity vector V without knowing the Doppler angle[38–40] and speckle analysis of structural (B-mode) OCT images, allowing velocity estimation without invoking the Doppler effect[41]. Also, signal processing techniques have been developed recently that lead to flow information extraction in spectral and frequency-swept OCT systems[13–18,42]. Thus, a variety of approaches exist to enable a researcher to detect blood flow with OCT, each with its own advantages and drawbacks. We now describe an example of time domain D-OCT flow imaging in some detail, in order to demonstrate the central concepts and outline the biomedical potential of Doppler OCT.

IMPLEMENTATION: EXAMPLE OF PHASE-RESOLVED TIME DOMAIN DOPPLER OCT SYSTEM BASED ON KASAI VELOCITY ESTIMATOR

Doppler US is an established field with many validated techniques for clinical imaging, and Doppler OCT, while differing from it in many respects, also shares considerable similarities. It is therefore useful to discuss Doppler OCT with reference to many mature concepts common in the US literature, and to explore the utility and benefit of their adoption into the OCT domain. A widely used velocity estimation method in Doppler ultrasound for real-time flow imaging was based on calculating the phase change between successive echoes from moving blood, as shown in 1982 by Namekawa *et al.*[43] Known as the Kasai estimator[44], this autocorrelation technique stemmed from radar research performed in the early 1950s, and was first described in the US literature in the 1970s[45]. Subsequently, this technique was developed into the first commercial color-flow Doppler US imaging system and gained wide clinical and commercial acceptance[25].

The basic setup required to perform time-domain D-OCT employing the Kasai technique is depicted in Figure 32.3, showing the in-phase and quadrature demodulator module after the basic OCT system.

The above implementation employs hardware demodulation to extract the in-phase (I) and quadrature (Q) components of the complex D-OCT signal, and then computes phase via a two-dimensional software-based Kasai algorithm (from which the Doppler shift, and then perhaps velocity, can be obtained if the Doppler angle(s) are known). Further, removal of background bulk tissue Doppler signal is incorporated into the system. The resulting frame rates, signal-to-noise ratio, velocity sensitivity and dynamic range can enable a variety of *in vivo* Doppler applications[46], as summarized below.

It is important to realize that there is no unique and optimum way to represent Doppler blood flow information. Therefore, multiple Doppler modes have been developed in clinical Doppler US systems, each with its own set of advantages and disadvantages; the most common ones include color Doppler, sonogram (also known as Doppler spectrum or Doppler waveform) and power Doppler modes. Analogous D-OCT modes of display can also be calculated from the digital I and Q signals furnished by the above setup. While I and Q are primarily used for phase estimation, as below, the structural images are obtained simultaneously by displaying in gray-scale the logarithm of $[I^2 + Q^2]^{1/2}$ at each pixel location.

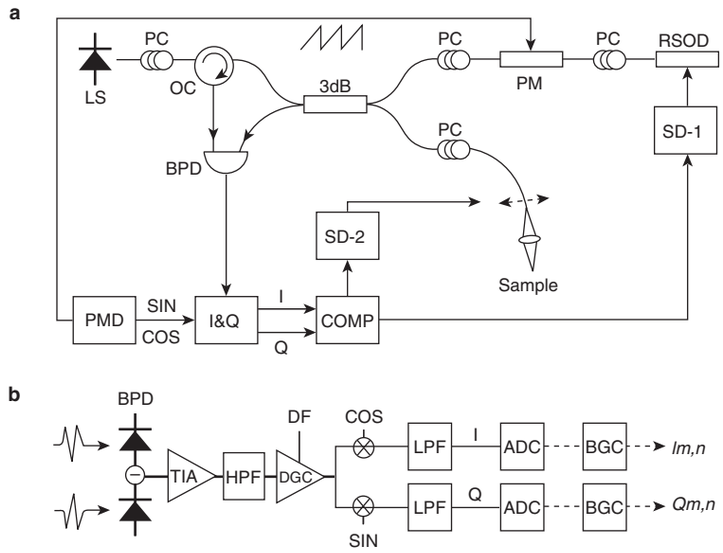

Figure 32.3 (a) Schematic diagram of the time-domain D-OCT system based on the Kasai velocity estimator method. LS, light source; PC, polarization controller; OC, optical circulator; 3dB, 50–50 fiber coupler; PM, phase modulator; RSOD, rapid scanning optical delay line; BPD, balanced photo-detector; PMD, phase modulator driver; I&Q, in-phase and quadrature demodulator; SD-1 and -2, scanner drivers; COMP, computer. (b) The hardware and software signal conditioning chain, particularly the I&Q demodulator. TIA, trans-impedance amplifier; HPF and LPF, high- and low-pass filters; DGC, depth-gain-compensation amplifier; DF, depth feedback signal; SIN and COS, 0° and 90° shifted carrier frequency, synchronized to the PMD; ADC, analog-to-digital converter; BGC, digital bias and gain compensation[46]

Color Doppler mode

The total mean velocity V at any pixel can be evaluated by the Kasai autocorrelation equation:

$$\langle v \rangle = \frac{\lambda_0 f_D}{2n_t \cos(\theta)}, \text{ and}$$

$$f_D = \frac{f_a}{2\pi} \arctan\left\{ \frac{\frac{1}{M(N-1)} \sum_{m=1}^{M} \sum_{n=1}^{N-1} (I_{m,n+1} Q_{m,n} - Q_{m,n+1} I_{m,n})}{\frac{1}{M(N-1)} \sum_{m=1}^{M} \sum_{n=1}^{N-1} (Q_{m,n+1} Q_{m,n} + I_{m,n+1} I_{m,n})} \right\} = \frac{f_a}{2\pi} \arctan\left\{ \frac{\langle Y \rangle}{\langle X \rangle} \right\} \quad (3)$$

where f_D is the Doppler frequency shift, n_t is the tissue index of refraction (~1.4), θ is the Doppler angle, m and n denote the indices in the depth and lateral directions, respectively, and Y, X will be used for estimating the variance of velocity estimate (see below). The phase estimation is performed within an $M \times N$ window to improve accuracy through averaging. The size of the window and the degrees of two-dimensional overlap are user-selectable and can be optimized based on desired frame rates, velocity estimation accuracy and spatial resolutions.

The resultant Doppler image information is usually displayed as a color map overlaid on the structural image, enabling simultaneous visualization of both tissue structure and functions as well as providing anatomical landmarks for flow information. As the Doppler angles are often unknown, especially in a complex three-dimensional geometry characteristic of tissue microcirculation, the velocity vectors are not calculated and the mean Doppler frequency shifts f_D at each pixel are displayed. Color Doppler is perhaps the most direct way to display blood flow information; one potential disadvantage of this mode is noise due to phase aliasing effects that occur at higher velocity flows (V_z > ~4 mm/s for the reported system with f_a ~8 kHz).

Doppler spectrum mode

Another clinically important display mode for Doppler ultrasound is the so-called sonogram or spectral (waveform) display, essentially a joint

time–frequency analysis of the flow signal using a transform method such as short-time Fast Fourier Transform (ST-FFT). The spectral display is usually calculated at a particular location within a blood vessel, often identified by color Doppler imaging, to illustrate the velocity (or Doppler frequency) distribution as a function of time. The Doppler spectrum of that location at time nT_a (T_a=1/f_a is the period for one axial scan) is calculated by FFT over a window length N_{FFT}:

$$\left|\hat{S}(f_D)_{nT_a,M}\right| = \frac{1}{M}\sum_{m=1}^{M}\left|FFT\{W[S(t)_{n-N_{FFT},n,m}]\}\right| \quad (4)$$

where $S(t)_{n-N_{FFT},n,m}$ is the complex OCT signal sequence from time $(n–N_{FFT})T_a$ to $n\ T_a$, M is the depth window length (called range gate length in US literature), and W is a window function. This display mode is especially useful for examining time-varying flow patterns such as pulsatile flow. Associated with the spectral display, an audio output of the Doppler frequency distribution is often presented to the physician in Doppler US. The possibility of audible output stems from the fortuitous fact that, for typical physiological flow velocities, the resulting Doppler frequency shifts are around the low kilohertz range (see Figure 32.1), and can thus be directly heard by the human ear. Audio presentation can also be accomplished in the D-OCT system[10,46].

Power Doppler mode

Another approach to flow mapping is power Doppler, in which the area under the Doppler spectrum (excluding the DC component due to stationary tissue, known as tissue clutter) is calculated:

$$P_D = \frac{1}{MN}\sum_{m=1}^{M}\sum_{n=1}^{N}(I'^2_{m,n} + Q'^2_{m,n}) \quad (5)$$

where I' and Q' are high pass filtered from I and Q using a digital filter to remove signal from bulk tissue. The resultant integrated power Doppler signal is related to the volume of moving blood within the imaging volume and results in the loss of blood velocity and directionality information[46,47]. Although popular in US, this mode turns out to be rather computationally intensive in D-OCT because of the complex nature of noise due to bulk tissue motion (see Velocity histogram method, below). It must therefore be computed during post-processing and does not appear well suited for D-OCT real-time imaging.

Velocity variance mode

The velocity variance (or standard deviation) mode is not typically used as a stand-alone display in Doppler US systems, but has gained some popularity in D-OCT[10,11,38,46,48]. If the color-Doppler calculation is performed, relatively little additional computation is required to obtain the velocity variance (or standard deviation) information. If S^* is the complex conjugate of the OCT signal S, then the normalized velocity variance is:

$$\frac{\sigma_v^2}{f_a^2} = \left(1 - \frac{MN\left|\sum_{m=1}^{M}\sum_{n=1}^{N-1} S_{m,n}S^*_{m,n+1}\right|}{M(N-1)\sum_{m=1}^{M}\sum_{n=1}^{N-1} S_{m,n}S^*_{m,n}}\right) = \left(1 - \frac{\sqrt{\langle X\rangle^2 + \langle Y\rangle^2}}{\langle S^2\rangle}\right) \quad (6)$$

This can be evaluated efficiently, since $<X>$, $<Y>$ and $<S^2>$ have all been calculated for the color Doppler and structural display modes. Velocity variance mapping eliminates aliasing and can greatly increase the velocity measurement range. Since variance generally increases from the laminar to the turbulent regime, this mode can detect areas of significant turbulence, such as flow near obstructions and bifurcations in vessels; it can also help distinguish true blood flow from bulk tissue motion (e.g. heart wall motion, which typically moves together and thus exhibits low velocity variance). As in the power Doppler imaging, however, blood flow orientation information is lost. However, by combining information from both the color Doppler and the variance modes, one can also display 'directional velocity variance' data, similar to the directional power Doppler mode in clinical US.

Velocity histogram method for motion artifact rejection

A major difficulty in Doppler imaging of tissue blood flow is the signal contamination by bulk tissue motion that also produces a (blood-unrelated) Doppler signal. Thus, direct application of any of the Doppler modes described above may give erroneous results due to other sources of motion, which would require signal processing to remove[6,34]. An alternative approach to isolate the blood Doppler signal is based on velocity histogram analysis[49]. The basic approach is to derive the distribution of mean Doppler frequency shifts along each depth scan line, using the color Doppler imaging approach. The most prominent peak with a narrow velocity distribution is then probably due to bulk tissue motion, and can be eliminated from further analysis. Note that this method can remove motion artifacts both faster and slower than the blood flow velocity. Figure 32.4 demonstrates the effective use of this technique for *in vivo* Doppler imaging. Details of implementation, performance and assumptions of this important component of tissue Doppler OCT imaging can be found in the original literature[46,49].

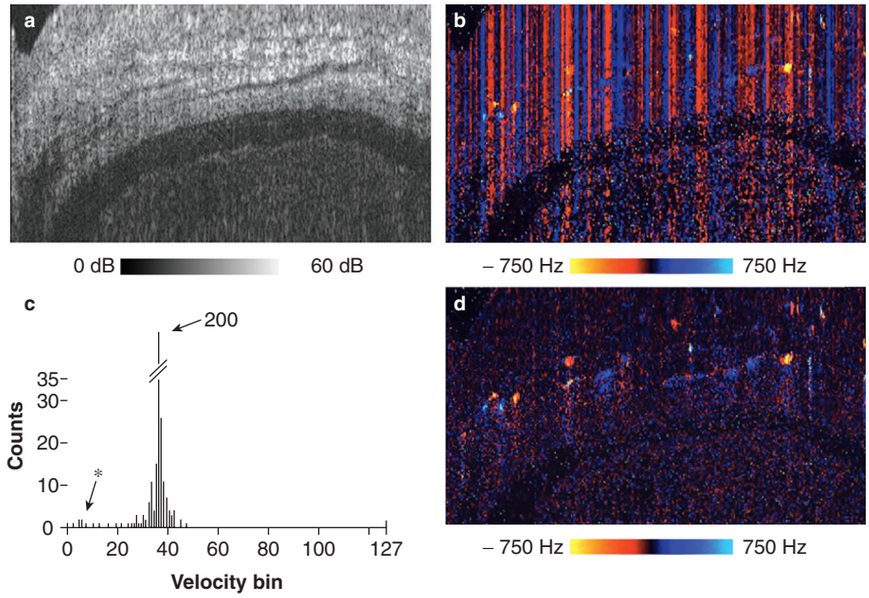

Figure 32.4 Cross-sectional *in vivo* D-OCT image of the human finger (dorsal skin surface above the nail root). Image size: 0.575 mm × 3 mm. (a) Structural image; (b) color Doppler image without motion artifact rejection; (c) a typical velocity histogram, showing the main peak with block tissue motion and the side band due to blood flow (*); (d) the corresponding color Doppler image with motion artifact rejection[49]

It is thus evident that different methods of flow detection, and different modes of flow analysis/display, are available for D-OCT. The time-domain Kasai-based D-OCT system described above can acquire, process and display data in real time at > 16 frames per second with 500 lines per image. At such frame rates, the histogram method for velocity noise filtering is applied in real time, and bidirectional color Doppler as well as velocity variance images are also displayed in real time. The methodology has enabled catheter-based D-OCT implementation for Doppler blood flow detection in endoscopic and interstitial settings, as illustrated below. The Kasai estimator can also be implemented in digital hardware to further improve the computation speed. It is likely that the continuing advances in spectral- and frequency-domain OCT will yield clinical systems with faster speeds and higher signal-to-noise ratio for Doppler imaging in these challenging clinical settings.

DOPPLER OCT BIOIMAGING WITH THE ABOVE IMPLEMENTATION

The following illustrative examples of various flow display modes in a variety of *in vivo* systems demonstrate the technological and clinical potential of Doppler imaging with OCT, using the time domain Kasai-based implementation described above. Figure 32.5 shows D-OCT imaging results for measuring steady flow in a rectangular flow phantom[46]. The scattering suspension of 0.25% Intralipid is flowing out of the page. The rings due to phase aliasing wrap-around

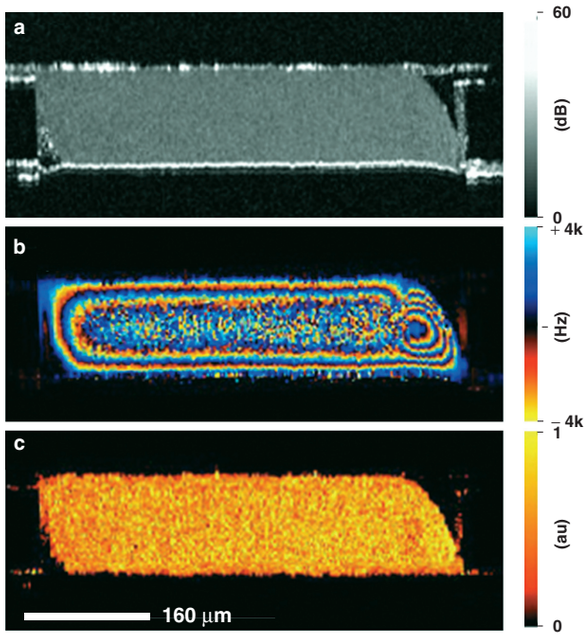

Figure 32.5 (a) Structural, (b) color Doppler, and (c) normalized power Doppler OCT images of a glass channel flow phantom of 0.25% Intralipid. Note the aliasing effect in (b) due to phase wrap-around, and the loss of flow directionality in (c)[46]

are clearly seen in the color Doppler image. The color codes for Doppler shifts are indicated on the scale bar, and are assigned to be blue for flow towards the observer and red for flow away from the observer in

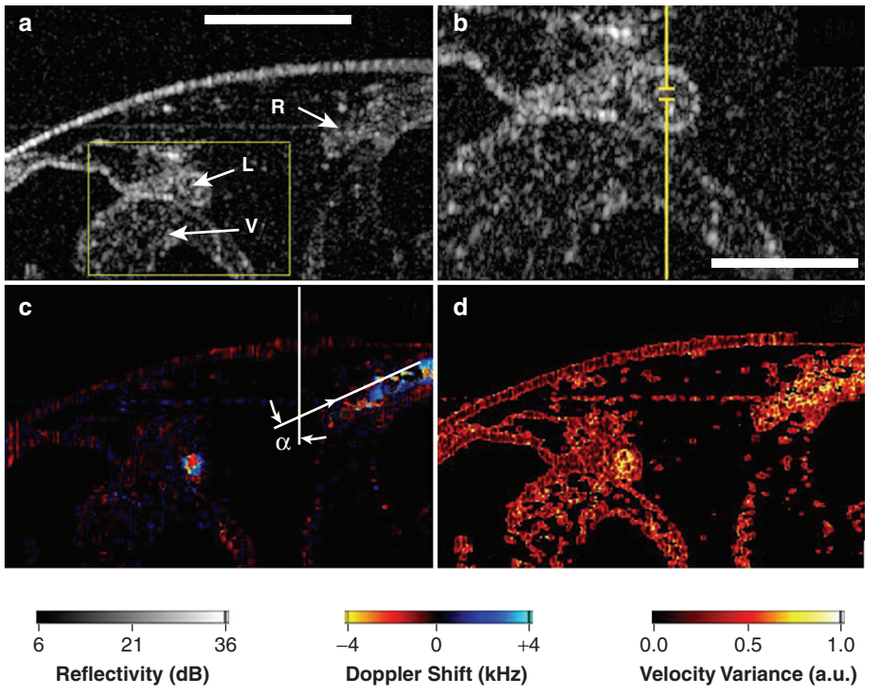

Figure 32.6 DOCT image of a *Xenopus* tadpole, imaging the left and right branches of the truncus arteriosis (L and R), acquired at 8 fps. (a) Structural (B-mode) image of the aortic branches cross-section. Notice a smaller vessel (V). Bar = 500 μm. (b) 2 × zoom of the yellow rectangular region in (a), showing the micro-structure of L. The break in the yellow line indicates the location from which Doppler spectrum information is collected and encoded into spectral (audio) format (see Figure 32.7), demonstrating the velocity distribution within L. Bar = 250 μm. (c) Color-Doppler image, showing the corresponding velocity map in the cross-section. The Doppler angle (α) is estimated to be ~ 63° for R. The small blood vessel (V) is much better visualized in the color-Doppler mode, allowing estimation of its diameter to be less than 70 μm. The peak Doppler shift is ~ 9 kHz considering aliasing effects. (d) Velocity variance image, showing the increased variance of the blood flow within L and R. Each individual image was recorded at 450 × 508 pixels[10]

accordance with the Doppler US convention. A region of flow disturbance, represented by an additional set of smaller aliasing rings, is also seen in the bottom right corner. The normalized power Doppler display removes this aliasing artifact, although the directional flow information is lost. Since the power Doppler mode does not measure flow velocity but indicates absence or presence of flow, the entire phantom cross section appears uniformly bright. This is in contrast to velocity variance image, which also loses directional flow information, but does appear brighter in the center corresponding to regions of higher velocity flow (further details in reference 46). Thus, in comparing the power Doppler with the velocity variance D-OCT modes, the latter is seen to be less computationally intensive while also regaining some of the velocity gradient information.

The cardiac dynamics of the *Xenopus laevis* tadpole as visualized by D-OCT, using a hand-held probe, are illustrated in Figure 32.6[46]. This important developmental biology model can be used to study the phenotypic expression of genetic abnormalities, normal embryonic development, structure–function relationships and longitudinal disease progression; it can also serve as a useful *in vivo* test bed for D-OCT system refinement and characterization. Shown in the figure are left and right branches of the truncus arteriosis leading to the three chambers of the tadpole heart. This view permits cross-sectional visualization of blood flow in the left branch, as well as determination of the Doppler angle in the right branch for absolute flow velocity calculations. The higher signal intensities in the velocity variance image corresponding to the locations of the vessels are clearly distinguishable from the adjacent lower-variance signals corresponding to heart wall motion. This, in combination with other D-OCT display modes and the histogram velocity filtering technique, allows one to detect the blood flow Doppler signal in the presence of other confounding tissue motions. The dynamic nature of the beating heart is better appreciated by viewing the associated videos, as contained in the original publication that supports multimedia formats[10].

The Doppler spectrum display corresponding to the left branch of the truncus arteriosis location is shown in Figure 32.7. The time-varying spectral distribution waveform clearly demonstrates the need for (and the ability of) fast D-OCT imaging, enabling

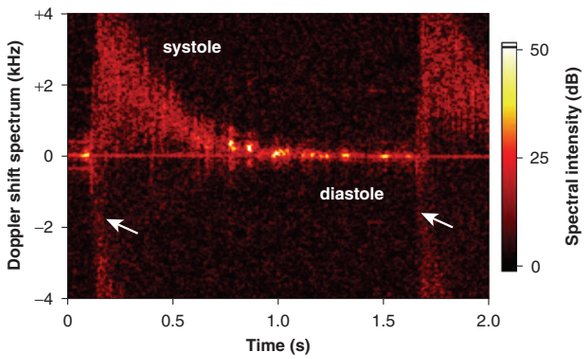

Figure 32.7 Doppler spectral display of the D-OCT system. The full Doppler spectrum represents the velocity distribution of the blood flowing within the analysis window, which is the gap in the yellow line shown in Figure 32.6(b). Notice the rapid onset of systole and the aliasing caused by the peak velocity (arrows), as well as the relatively longer time for diastole (heart relaxation)[10]

the temporal capture of both systole and diastole events in the rapidly beating tadpole heart. Again, the reader is referred to the original multimedia publication for more complete video and audio representations of the cardiac dynamics[10].

One of the major limitations of OCT is its shallow depth of imaging, limited to 1–3 mm in most tissues because of the extensive tissue scattering. While this depth is probably adequate for a variety of applications, such as studies of skin, epithelial linings of body orifices (e.g. gastrointestinal tract) and intravascular structures, deeper tissues and organs are difficult to access by OCT. One method to partially overcome this limitation is to image at the tip of a fine needle that can be inserted deep into tissue to the desired location[50,51]. This methodology can be engineered into a sub-millimeter-diameter imaging probe capable of imaging bidirectional blood flow and microstructure several centimeters deep into the tissue. Figure 32.8 demonstrates proof-of-principle Doppler imaging capability of this approach when applied to Doppler OCT[52]. The small size of the probe, its visualization and guidance by conventional imaging modalities (US, X-rays), and the high-quality structural and functional blood flow information afforded by the interstitial approach will be likely to expand the range of anatomical sites and clinical/research scenarios accessible to D-OCT.

To conclude this section of illustrative examples of D-OCT imaging *in vivo*, Figures 32.9 and 32.10 display the results of microvascular blood flow detection in the superficial layers of the human gastrointestinal tract, performed during routine esophageal endoscopy in the clinic[12,46]. It should be noted that endoscopic D-OCT represents a significant technological challenge. The small size of the blood vessels, the slow blood velocities, and the relative motion between the distal imaging tip and the gastrointestinal tissue (caused by the mechanics of the imager, the motion of the endoscope, or the physiology of the patient) demand a D-OCT system with high-velocity sensitivity and a robust noise-suppression algorithm, all while remaining compatible with the temporal and spatial constraints of a clinical endoscopy suite. If successful, however, the addition of Doppler blood flow information to previously reported high-resolution microstructural gastrointestinal OCT imaging may prove valuable for vascular diagnosis, early disease detection, disease prognosis and real-time assessment of local therapies. The results in normal esophagus (Figure 32.9) and in a pre-neoplastic condition known as Barrett's esophagus (Figure 32.10) demonstrate the clinical feasibility of blood flow detection in human gastrointestinal tissues during routine endoscopy. It was found that, in addition to differing microstructures, normal and diseased gastrointestinal tissues demonstrate different mucosal/submucosal microcirculation patterns. The scientific and clinical utility of this D-OCT finding is currently being evaluated.

SUMMARY

Accurate assessment of blood flow in tissues is important in biomedicine. It has been said that 'where blood does not flow, life does not go', and that assertion underscores the importance of hemodynamics that can benefit from non-invasive high-resolution imaging of the blood flow, especially at the microvascular level. This importance is further highlighted in oncological applications with the recent emphasis on tumor vasculature, angiogenic processes and developments of antiangiogenic therapies in combating the cancer burden. While a variety of medical imaging modalities have been developed for blood flow imaging in the body, including ultrasound, MRI and CT, none can directly image microvascular blood flow in intact tissues. D-OCT, with its ability to simultaneously furnish structural and functional images with micrometer-scale spatial resolution and sub-mm/s blood flow sensitivity up to a depth of ~2 mm in most mammalian tissues, can thus fill a useful niche in medical imaging for blood flow detection. D-OCT's particular strengths – its high imaging speed, non/minimally invasive nature, affordability, robustness, portability, wide velocity dynamic range, and exceptionally high spatial and velocity resolution – can be advantageously exploited in various clinical scenarios. In addition to selected areas highlighted in this monogram, detailed knowledge of *in vivo* blood flow is important for studies of ocular (retinal) hemodynamics, burn depth estimation, assessment of viability of transplanted tissue viability, laser treatment planning of port wine stains,

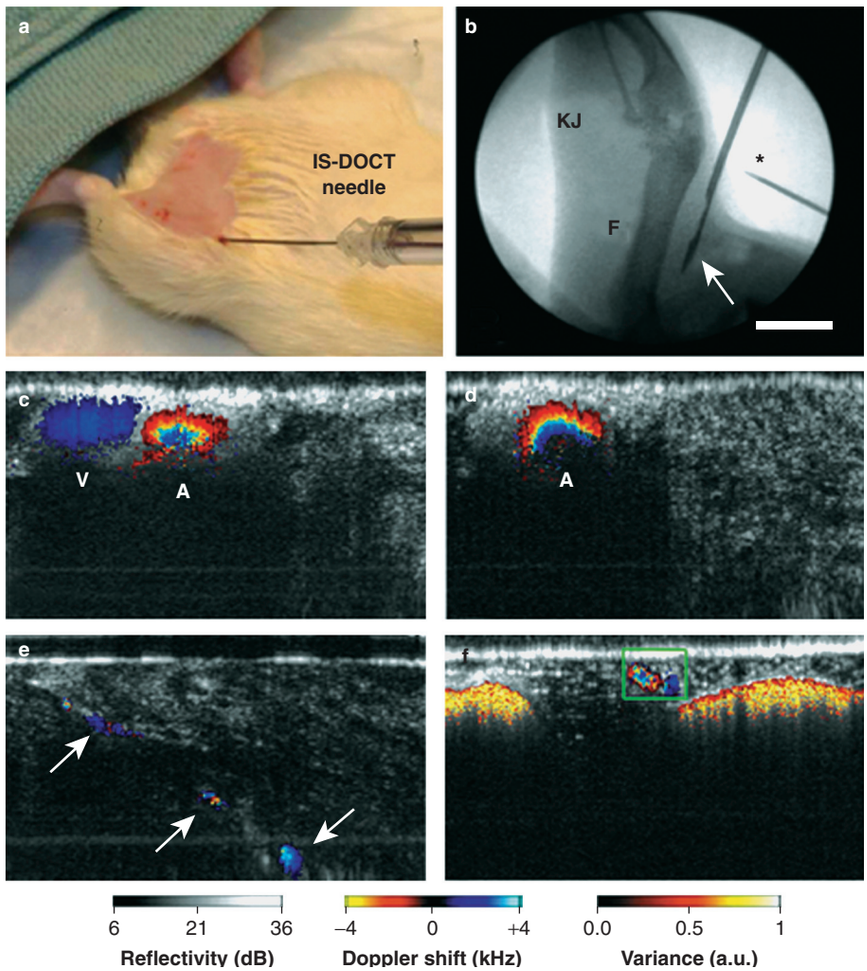

Figure 32.8 *In vivo* demonstration of interstitial D-OCT. (a) The needle probe inserted in the thigh of an anesthetized rat. (b) Fluoroscopy showing the needle position (arrow) with relation to the femur (F) and knee joint (KJ). Another needle tip (*) marked the surface of the skin, showing that the needle was ~15 mm into the tissue. (Scale bar = 1mm). (c) Interstitial-D-OCT image of an artery (A)–vein (V) pair, probably the femoral profunda of the rat. The flow velocity in the artery was higher, as shown by the aliasing effect. The venous flow could be obliterated by compressing the vessel (see d). (e) Smaller blood vessels (arrows: diameter ~ 100 μm) were detected in the rat gluteal muscle. (f) In rat abdomen, both small and large blood vessels were detected. Due to the large velocity differences in these vessels, the larger vessels were shown with velocity variance color scale, while the smaller vessels were shown with Doppler shift color scale (green window). Imaging depth was reduced beneath large blood vessels, probably due to blood attenuation of the signal. Interstitial D-OCT image dimension: 2.5 mm × 1.5 mm

treatment response monitoring and optimization for a variety of therapies (PDT, chemotherapy, radiation therapy), determination of flow abnormalities associated with occlusive vascular disease, embryological and developmental biology studies of angiogenesis (in both wild-type and transgenic models), assessment of bleeding risks of superficial vasculature and longitudinal studies of microvascular development in neoplastic transformations.

Further improvements in Doppler OCT methods, including, dynamic focusing, coherence gate focus tracking with a microelectromechanical mirror (MEMS)[53,54], expanding use of spectral- and frequency-domain D-OCT approaches[13–18,55], development of flow and structural (molecular) contrast agents[56,57] and quantification of blood flow metrics as surrogate markers for a particular indication may further enhance the adoption of this promising technology into the biomedical imaging armamentarium.

ACKNOWLEDGMENTS

We sincerely thank our many friends and colleagues in the field of biomedical optics, both in Canada and abroad, particularly those in OCT research. The valuable contributions of collaborating scientists, clinicians, engineers, machinists, nurses, clinical fellows and the many students and post-doctoral fellows are gratefully acknowledged. Our OCT research is

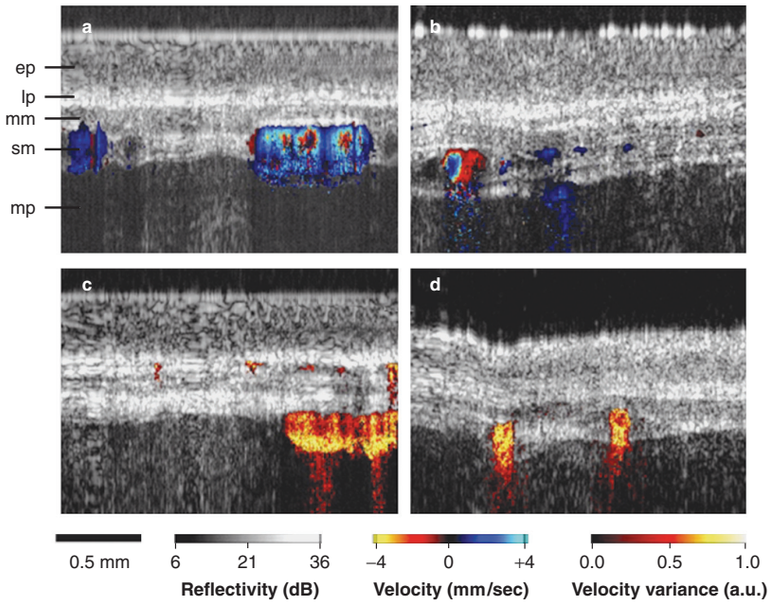

Figure 32.9 Human endoscopic D-OCT images of normal esophagus with the five layers indicated: epithelium (ep), lamina propria (lp), muscularis mucosa (mm), submucosa (sm) and muscularis propria (mp). (a and b) Color Doppler images showing vessels of microcirculation in the muscularis mucosa, submucosa and muscularis propria. The color rings in the larger vessels were caused by aliasing, due to the flow velocity exceeding the maximum detection range (±4 mm/s). (c and d) Velocity-variance images of the microcirculation in the lamina propria, muscularis mucosa, submucosa and muscularis propria. Note that few blood vessels were observed in the epithelium. The probe was in contact with the epithelial surface and the compression flattened the epithelium in (a) and (c)[12]

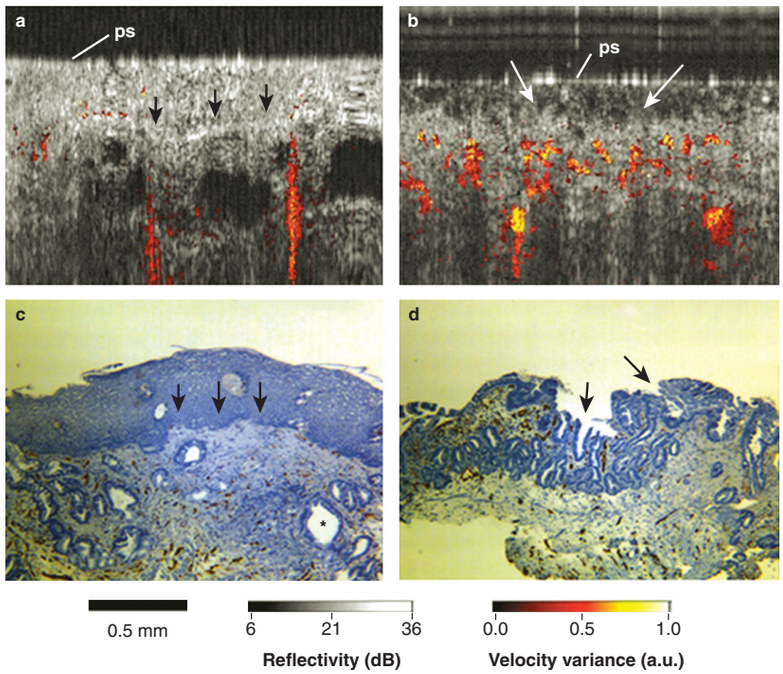

Figure 32.10 Velocity-variance endoscopic D-OCT images of Barrett's esophagus (BE) from two different patients, and histological comparison. (a and c) Sub-squamous BE with mucosal glands underneath the clearly delineated epithelium–lamina propria interface (arrows). Note the microvasculature surrounding the glands indicated by the velocity variance signal in (a) and by vascular staining using CD34 stain (dark brown) in (c), which was not observed in normal esophagus. The probe surface (ps) was in contact with the squamous epithelium. (b and d) BE with superficial glandular structure (arrows) and microvasculature close to the surface. Note the lack of distinct normal layers. Diffuse patterns of blood vessels are seen, consistent with the CD34 staining[12]

supported by the Natural Sciences and Engineering Research Council of Canada, Canadian Institutes of Health Research, Ontario Research and Development Challenge Fund, Photonics Research Ontario, Premier's Research Excellence Award, and donations from the Gordon Lang and Samuel B. McLaughlin Foundations.

REFERENCES

1. Wang XJ, Milner TE, Nelson JS. Characterization of fluid flow velocity by optical Doppler tomography. Opt Lett 1995; 20: 1337–9
2. Izatt JA, Kulkarni MD, Yazdanfar S, et al. In vivo bidirectional color Doppler flow imaging of picoliter blood volumes using optical coherence tomography. Opt Lett 1997; 22: 1439–41
3. Chen Z, Milner TE, Digant D, Nelson SJ. Optical Doppler tomographic imaging of fluid flow velocity in highly scattering media. Opt Lett 1997; 22: 64–6
4. Yazdanfar S, Rollins AM, Izatt JA. Imaging and velocimetry of the human retinal circulation with color Doppler optical coherence tomography. Opt Lett 2000; 25: 1448–50
5. Yazdanfar S, Rollins AM, Izatt JA. In vivo imaging of human retinal flow dynamics by color Doppler optical coherence tomography. Arch Ophthalmol 2003; 121: 235–9
6. Zhao Y, Brecke KM, Ren H, et al. Three-dimensional reconstruction of in vivo blood vessels in human skin using phase-resolved optical Doppler tomography. IEEE J Sel Top Quantum Elec 2001; 7: 931–5
7. Westphal V, Yazdanfar S, Rollins AM, Izatt JA. Real-time, high velocity-resolution color Doppler optical coherence tomography. Opt Lett 2002; 27: 34–6
8. Milner TE, Yasdanfar S, Rollins AM, et al. Doppler optical coherence tomography In: Bouma BE, Tearney GJ, eds. Handbook of Optical Coherence Tomography. New York: Marcel Dekker, 2002: 203–36
9. Rollins AM, Yazdanfar S, Radhakrishnan S, et al. Real-time imaging of microstructure and blood flows using optical coherence tomography. In: Tuchin V, ed. Handbook of Biomedical Optics. Bellingham: SPIE Press, 2003: 939–86
10. Yang VXD, Gordon ML, Qi B, et al. High speed, wide velocity dynamic range Doppler optical coherence tomography (part II): imaging in vivo cardiac dynamics of Xenopus laevis. Opt Express 2003; 11: 1650–8
11. Yang VXD, Gordon ML, Tang S, et al. High speed, wide velocity dynamic range Doppler optical coherence tomography (part III): in vivo endoscopic imaging of blood flow in the rat and human gastrointestinal tract. Opt Express 2003; 11: 2416–24
12. Yang VXD, Tang S, Gordon ML, et al. Endoscopic Doppler optical coherence tomography in the human GI tract: initial experience. Gastrointest Endosc 2005; 61: 879–90
13. White BR, Pierce MC, Nassif N, et al. In vivo dynamic human retinal blood flow imaging using ultra-high-speed spectral domain optical Doppler tomography. Opt Express 2003; 11: 3490–7
14. Leitgeb RA, Schmetterer L, Drexler W, et al. Real-time assessment of retinal blood flow with ultra fast acquisition by color Doppler Fourier domain optical coherence tomography. Opt Express 2003; 11: 3116–21
15. Park BH, Pierce MC, Cense B, et al. Real-time fiber-based multi-functional spectral-domain optical coherence tomography at 1.3 μm. Opt Express 2005; 13: 3931–44
16. Ren H, Sun T, MacDonald DJ, et al. Real-time in vivo blood flow imaging by moving scatterer sensitive spectral domain optical Doppler tomography. Opt Lett 2006; 31: 927–9
17. Zhang J, Chen ZP. In vivo blood flow imaging by a swept source based Fourier domain optical Doppler tomography. Opt Express 2005; 13: 7449–57
18. Vakoc BJ, Yun SH, de Boer JF, et al. Phase-resolved optical frequency domain imaging. Opt Lett 2005; 13: 5483–93
19. Lunde OC. Evaluation of endoscopic laser Doppler flowmetry for measurement of human gastric blood flow: methodological aspects. Scand J Gastroenterol 1988; 23: 1072–8
20. Chauhan BC, Smith FM. Confocal scanning laser Doppler flowmetry: experiments in a model flow system. J Glaucoma 1997; 6: 237–45
21. Wardell K, Nilsson G. Laser Doppler imaging of the skin In: Serup J, Jemec GBE, eds. Handbook of Non-Invasive Methods and the Skin. Boca Raton: CRC Press, 1995: 421–8
22. Aspres N, Egerton I, Lim A. Imaging the skin. Australas J Derm 2003; 44: 19–27
23. Nicolela MT, Hnik P, Schulzer M, Drance SM. Reproducibility of retinal and optic nerve head blood flow measurements with scanning laser Doppler flowmetry. J Glaucoma 1997; 6: 157–64
24. Schilling MK, Redaelli C, Freiss H, et al. Evaluation of laser Doppler flowmetry for the study of benign and malignant gastric blood flow in vivo. Gut 1999; 45: 341–5
25. Jensen JA. Estimation of Blood Velocities Using Ultrasound: a Signal Processing Approach. Cambridge: Cambridge University Press, 1996
26. Rubin JM, Bude RO, Carson PL, et al. Power Doppler ultrasound: a potentially useful alternative to mean frequency based color Doppler. Radiology 1994; 190: 853–6
27. Powers JE, Burns PN, and Souquet J. Imaging instrumentation for ultrasound contrast agents. In: Nanda NC, Reinhard S, Goldberg BB, eds. Advances in Echo Imaging Using Contrast Enhancement. Dordrecht, Netherlands: Kluger Academic Press, 1997
28. Loupas T, Powers JE, Gill RW. An axial velocity estimator for ultrasound blood flow imaging based on the full evaluation of the Doppler equation using a 2-dimensional autocorrelation approach. IEEE Trans Ultrason Ferroelec Freq Contr 1995; 42: 672–88
29. Foster FS, Pavlin CJ, Harasiewicz KA, et al. Advances in ultrasound microscopy. Ultrasound Med Biol 2000; 26: 1–27
30. Goertz DE, Christopher DA, Yu JL, et al. High-frequency color flow imaging of the microcirculation. Ultrasound Med Biol 2000; 26: 63–71
31. Goertz DE, Yu JL, Kerbel RS, et al. High-frequency Doppler ultrasound monitors the effects of antivascular therapy on tumor blood flow. Cancer Res 2002; 62: 6371–5

32. Fung YC. Biomechanics of Microcirculation, 2nd edn. New York: Prentice Hall, 1997
33. Kulkarni MD, van Leeuwen TG, Yazdanfar S, Izatt JA. Velocity estimation accuracy and frame rate limitations in color Doppler optical coherence tomography. Opt Lett 1998; 23: 1057–9
34. Chen Z, Zhao Y, Srinivas SM, et al. Optical Doppler tomography. IEEE J Sel Top Quantum Electron 1999; 5: 1134–41
35. Zhao Y, Chen Z, Saxer C, et al. Phase-resolved optical coherence tomography and optical Doppler tomography for imaging blood flow in human skin with fast scanning speed and high velocity sensitivity. Opt Lett 2000; 25: 1358–60
36. Pierce MC, Park BH, Cense B, de Boer JF. Simultaneous intensity, birefringence, and flow measurements with high speed fiber-based optical coherence tomography. Opt Lett 2002; 27: 1534–6
37. Chen Z, Milner TE, Srinivas S, et al. Noninvasive imaging of in vivo blood flow velocity using optical Doppler tomography. Opt Lett 1997; 22: 1119–21
38. Proskurin SG, He Y, Wang RK. Determination of flow velocity vector based on Doppler shift and spectrum broadening with optical coherence tomography. Opt Lett 2003; 28: 1227–9
39. Wu L. Simultaneous measurement of flow velocity and Doppler angle by the use of Doppler optical coherence tomography. Opt Laser Eng 2004; 42: 303–13
40. Piao D, Quing Z. Direct bidirectional angle-insensitive imaging of the flow signal intensity in Doppler optical coherence tomography. Appl Opt 2005; 44: 348–57
41. Barton JK, Stromski S. Flow measurement without phase information in optical coherence tomography images. Opt Express 2005; 13: 5234–9
42. Leitgeb RA, Schmetterer L, Hitzenberger CK, et al. Real-time measurement of in vitro flow by Fourier-domain color Doppler optical coherence tomography. Opt Lett 2004; 29: 171–3
43. Namekawa K, Kasai C, Tsukamoto M, Koyano A. Real-time blood flow imaging system utilizing auto-correlation techniques In: Lerski RA, Morley P, eds. Proceedings of Ultrasound' 82. New York: Pergamon Press, 1982: 203–8
44. Kasai C, Namekawa K, Koyano A, Omoto R. Real-time two-dimensional blood flow imaging using an auto-correlation technique. IEEE Trans Son Ultrason 1985; 32: 458–63
45. Grandchamp PA. A novel pulsed directional Doppler velocimeter: the phase detection profilometer. In: Kazner E, de Vieger M, Muller RH, McCready VR, eds. Ultrasonics in Medicine. (Proceedings of the 2nd European Congress). Amsterdam: Excerpta Medica, 1975: 137–143
46. Yang VXD, Gordon ML, Qi B, et al. High speed, wide velocity dynamic range Doppler optical coherence tomography (part I): system design, signal processing, and performance characterization. Opt Express 2003; 11: 794–809
47. Ren H, Wang Y, Nelson JS, et al. Power optical Doppler tomography imaging of blood vessels in human skin and M-mode Doppler imaging of blood flow in chick chrioallantoic membrane. Proceedings of SPIE 2003; 225–31
48. Zhao Y, Chen Z, Saxer C, et al. Doppler standard deviation imaging for clinical monitoring of in vivo human skin blood flow. Opt Lett 2000; 25: 114–16
49. Yang VXD, Gordon ML, Mok A, et al. Application of the Kasai velocity estimator and histogram segmentation for resolution improvement and motion suppression in phase-resolved optical Doppler tomography. Opt Commun 2002; 208: 209–14
50. Li XD, Chudoba C, Ko T, et al. Imaging needle for optical coherence tomography. Opt Lett 2000; 25: 1520–2
51. Reed WA, Yan MF, Schnitzer MJ. Gradient-index fiber-optic microprobes for minimally invasive in vivo low-coherence interferometry. Opt Lett 2002; 27: 1794–6
52. Yang VXD, Mao YX, Munce N, et al. Interstitial Doppler optical coherence tomography. Opt Lett 2005; 30: 1791–3
53. Qi B, Himmer PA, Gordon ML, et al. Dynamic focus control in high-speed optical coherence tomography based on a microelectromechanical (MEMS) mirror. Opt Commun 2004; 232: 123–8
54. Yang VX, Mao Y, Standish B, et al. Doppler optical coherence tomographys with micro-electro-mechanical membrane mirror for high-speed dynamic focus tracking. Opt Lett 2006; 31: 1262–4
55. Wojtkowski M, Bajraszewski T, Targowski P, Kowalczyk A. Real-time in vivo imaging by high-speed spectral optical coherence tomography. Opt Lett 2003; 28: 1745–7
56. Barton JK, Hoying JB, Sullivan CJ. Use of microbubbles as an optical coherence tomography contrast agent. Acad Radiol 2002; 9: S52–5
57. Yang C. Molecular contrast optical coherence tomography: a review. Photochem Photobiol 2005; 81: 215–37